All deformation potentials in GaN determined by reflectance spectroscopy under uniaxial stress: Definite breakdown of the quasicubic approximation

AUTHOR(S):

Ishii, Ryota; Kaneta, Akio; Funato, Mitsuru; Kawakami, Yoichi

CITATION:

Ishii, Ryota ...[et al]. All deformation potentials in GaN determined by reflectance spectroscopy under uniaxial stress: Definite breakdown of the quasicubic approximation. Physical Review B 2010, 81(15): 155202.

ISSUE DATE:

2010-04

URL:

http://hdl.handle.net/2433/128922

PHYSICAL REVIEW B **81**, 155202 (2010)

All deformation potentials in GaN determined by reflectance spectroscopy under uniaxial stress: Definite breakdown of the quasicubic approximation

Ryota Ishii,* Akio Kaneta, Mitsuru Funato, and Yoichi Kawakami†
Department of Electronic Science and Engineering, Kyoto University, Kyoto 615-8510, Japan

Atsushi A. Yamaguchi
Research Laboratory for Integrated Technological Systems, Kanazawa Institute of Technology, Tokyo 105-0002, Japan
(Received 7 December 2009; revised manuscript received 1 March 2010; published 8 April 2010)

Reflectance spectroscopy was performed for nonpolar and semipolar bulk GaN substrates under uniaxial stress. The exciton-transition energies and oscillator strengths clearly depended on uniaxial stress. The results were interpreted by group theory on excitons and analyzed in terms of the effective Hamiltonian proposed by Bir and Pikus. In the Hamiltonian, the short-range Coulomb interaction was taken into consideration. This approach allows all exciton deformation potentials to be determined without the quasicubic approximation and we found that the exciton deformation potentials in GaN considerably deviate from the quasicubic approximation.

DOI: 10.1103/PhysRevB.81.155202 PACS number(s): 71.70.Fk, 71.55.Eq, 71.35.−y

I. INTRODUCTION

GaN-related materials have received much attention for optoelectronic applications because they interact with photons in the ultraviolet to near-infrared region. Highly efficient light-emitting diodes and high-power laser diodes (LDs) have been realized in the blue and blue-green regions using InGaN quantum wells (QWs).[1]

However, the external quantum efficiency of *c*-plane (polar plane) InGaN QWs decreases rapidly as the In composition increases due to the quantum-confined Stark effect caused by the piezoelectric polarization and degradation of the crystal quality.[2] Under these circumstances, a reduction in the piezoelectric polarization in nonpolar and semipolar planes has been theoretically predicted,[3,4] and is consistent with the experimental observation of fast radiative recombination lifetimes compared to those for polar plane.[5,6] Recently, many groups including ours have reported crystal growth and device fabrications onto these nonpolar and semipolar planes.[7–10] Moreover, green LDs operating at 520 nm at room temperature in the continuous-wave mode have been realized on the $\{20\bar{2}1\}$ plane.[11] To fully understand the device performances and to create novel functionalities, it is indispensable to understand the electronic band structures of nonpolar and semipolar QWs.

It has been theoretically predicted that anisotropic strain will drastically alter the electronic band structures of strained nonpolar and semipolar InGaN or AlGaN QWs.[3,12–14] Additionally, a very interesting physical phenomenon, polarization switching was theoretically predicted.[15] Then, our group[16] has experimentally observed polarization switching in $(11\bar{2}2)$ plane InGaN QWs with high In compositions and we noted the importance of strain. However, the analyses in the aforementioned papers relied on the accuracy of GaN physical parameters such as the deformation potentials. Therefore, to fully understand fundamental physics and to optimize device performance, a comprehensive study about the strain-induced effects in GaN-related materials is necessary.

It has been demonstrated that deformation potential theory can well explain the influence of strain on the electronic band structure.[17,18] In this theory, strain-induced effects are completely determined by the exciton deformation potentials. To date, nearly all papers have experimentally determined exciton deformation potentials in GaN using a combination of x-ray measurements with optical measurements on heteroepitaxial *c*-plane GaN films.[19–25] However, errors are unavoidable in these estimated values due to strain inhomogeneity. Furthermore, the quasicubic approximation must be used to extract all the exciton deformation potentials because this approach gives only a part of the exciton deformation potentials or the relations between them.[18] On the other hand, optical measurements under uniaxial stress are very suitable measurement techniques which can create various strained environments. Such techniques have yielded the exciton deformation potentials of II-VI compounds such as ZnO, CdS, and CdSe without the quasicubic approximation.[26–29] For *c*-plane GaN thin films grown on sapphire, Yamaguchi *et al.*[30] have demonstrated reflectance spectroscopy under uniaxial stress. However, the relatively large linewidth due to the heteroepitaxial growth prevented the C-exciton transition (Hopfield notation)[31] from being resolved, and furthermore, all the exciton deformation potentials have not been experimentally obtained because the uniaxial stress was applied only perpendicular to *c*-axis.

Herein, reflectance spectroscopy is performed for nonpolar and semipolar bulk GaN substrates under uniaxial stress along various directions. The experimental results are interpreted by group theory on excitons and analyzed in terms of the effective Hamiltonian where the short-range Coulomb interaction was taken into consideration. This approach allows us to determine all the exciton deformation potentials without the quasicubic approximation and we found that the exciton deformation potentials in GaN considerably deviate from the quasicubic approximation. Finally, we proposed a set of material parameters such as the crystal-field interaction, the spin-orbit interaction, the spin-exchange interaction, and the exciton deformation potentials in GaN.

TABLE I. Valence-electron and conduction-electron matrix at the Γ point. [$F_{\pm}=\Delta_1+\Delta_2+C_1\epsilon_{zz}+C_2(\epsilon_{xx}+\epsilon_{yy})+C_3\epsilon_{zz}+C_4(\epsilon_{xx}+\epsilon_{yy})\pm\frac{1}{2}j$; $G_{\pm}=\Delta_1-\Delta_2+C_1\epsilon_{zz}+C_2(\epsilon_{xx}+\epsilon_{yy})+C_3\epsilon_{zz}+C_4(\epsilon_{xx}+\epsilon_{yy})\pm\frac{1}{2}j$; $\lambda_{\pm}=C_1\epsilon_{zz}+C_2(\epsilon_{xx}+\epsilon_{yy})\pm\frac{1}{2}j$; $K=-C_5(\epsilon_{xx}-\epsilon_{yy}-2i\epsilon_{xy})$; and $H=-C_6(\epsilon_{xz}-i\epsilon_{yz})$.]

	$p_+\alpha\alpha$	$p_-\alpha\alpha$	$p_z\beta\alpha$	$p_+\beta\beta$	$p_-\beta\beta$	$p_z\alpha\beta$	$p_+\alpha\beta$	$p_-\alpha\beta$	$p_z\beta\beta$	$p_+\beta\alpha$	$p_-\beta\alpha$	$p_z\alpha\alpha$
$p_+\alpha\alpha$	F_-	K	0	$-j$	0	0	0	0	0	0	0	H
$p_-\alpha\alpha$	K^*	G_-	$\sqrt{2}\Delta_3$	0	$-j$	0	0	0	0	0	0	$-H^*$
$p_z\beta\alpha$	0	$\sqrt{2}\Delta_3$	λ_+	0	0	0	0	0	0	H^*	$-H$	0
$p_+\beta\beta$	$-j$	0	0	G_-	K	$\sqrt{2}\Delta_3$	0	0	H	0	0	0
$p_-\beta\beta$	0	$-j$	0	K^*	F_-	0	0	0	$-H^*$	0	0	0
$p_z\alpha\beta$	0	0	0	$\sqrt{2}\Delta_3$	0	λ_+	H^*	$-H$	0	0	0	0
$p_+\alpha\beta$	0	0	0	0	0	H	F_+	K	0	0	0	0
$p_-\alpha\beta$	0	0	0	0	0	$-H^*$	K^*	G_+	$\sqrt{2}\Delta_3$	0	0	0
$p_z\beta\beta$	0	0	0	H^*	$-H$	0	0	$\sqrt{2}\Delta_3$	λ_-	0	0	$-j$
$p_+\beta\alpha$	0	0	H	0	0	0	0	0	0	G_+	K	$\sqrt{2}\Delta_3$
$p_-\beta\alpha$	0	0	$-H^*$	0	0	0	0	0	0	K^*	F_+	0
$p_z\alpha\alpha$	H^*	$-H$	0	0	0	0	0	0	$-j$	$\sqrt{2}\Delta_3$	0	λ_-

II. THEORY

In this section, the effective exciton Hamiltonian in hexagonal symmetry[28] is described using notations in Ref. 32. We expanded this theory to obtain oscillator strengths for arbitrary directions. This procedure is essential for describing the optical properties of wurtzite materials grown on semipolar planes.

According to the effective Hamiltonian formalism proposed by Bir and Pikus,[18] the exciton Hamiltonian can be written as

$$H = H_c^0 + H_v^0 + H^{\text{strain}} + H^{\text{exciton}}, \tag{1}$$

where H_c^0 and H_v^0 are the nonstrain conduction and valence-band Hamiltonian, respectively. H^{strain} is a strain-related term. H^{exciton} originates from essentially two particle natures and is written as

$$H^{\text{exciton}} = \text{B.E.} + \frac{1}{2}j(\sigma_e \cdot \sigma_h), \tag{2}$$

where B.E. describes the exciton binding energy and j is the spin-exchange interaction constant which describes the electron-hole exchange interaction.[33]

Considering a hexagonal symmetry, Eq. (1) can be rewritten by the invariant method as

$$\begin{aligned} H^{\text{Wurtzite}} &= \Delta_1 J_z^2 + \Delta_2 J_z \sigma_{vz} + \Delta_3(\sigma_{+v}J_- + \sigma_{-v}J_+) \\ &+ (C_1 + C_3 J_z^2)\epsilon_{zz} + (C_2 + C_4 J_z^2)(\epsilon_{xx} + \epsilon_{yy}) \\ &- C_5(J_-^2\epsilon_+ + J_+^2\epsilon_-) - 2C_6([J_zJ_+]\epsilon_{-z} + [J_zJ_-]\epsilon_{+z}) \\ &+ \text{B.E.} + \frac{1}{2}j(\sigma_e \cdot \sigma_h), \end{aligned} \tag{3}$$

where

$$\epsilon_{\pm} = \epsilon_{xx} - \epsilon_{yy} \pm 2i\epsilon_{xy}, \quad \epsilon_{\pm z} = \epsilon_{xz} \pm i\epsilon_{yz} \tag{4}$$

and

$$C_1 = D_1 - a_{cz}, \quad C_2 = D_2 - a_{ct}, \quad C_3 = D_3, \quad C_4 = D_4,$$
$$C_5 = D_5, \quad C_6 = D_6. \tag{5}$$

Here J and σ describe the orbital angular momentum and Pauli-matrix operator, respectively, and their definitions are the same as those in Ref. 28. Δ_1 describes the crystal-field interaction due to the uniaxial crystal while Δ_2 and Δ_3 describe the spin-orbit interaction parallel and perpendicular to the c axis, respectively. C_i describes the exciton deformation potentials, which are related to the conduction-band deformation potentials (a_{cz}, a_{ct}) and the valence-band deformation potentials D_i by Eq. (5). ϵ_{ij} represents strain tensors. It should be noted that herein a negative sign indicates compressive strain, and we assumed that B.E. and Δ_{1-3} are strain independent.[34]

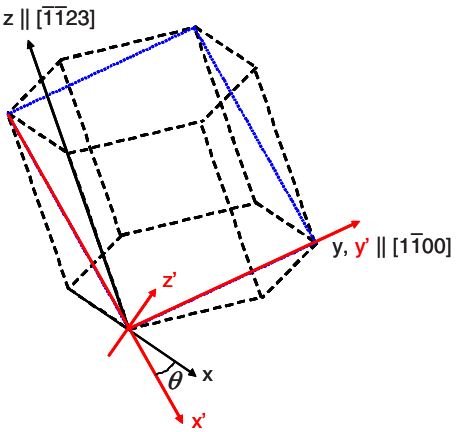

FIG. 1. (Color online) Relationship between (x,y,z) and (x',y',z') coordinates. Case for $(11\bar{2}2)$ plane is shown.

Considering that the conduction bands are s-like and the valence bands are p-like, general exciton wave functions can be written by a linear combination of the basis functions as

$$\begin{aligned}|\Psi^{\text{exciton}}\rangle = {} & a_1|p_+\alpha\alpha\rangle + a_2|p_-\alpha\alpha\rangle + a_3|p_z\beta\alpha\rangle + a_4|p_+\beta\beta\rangle \\ & + a_5|p_-\beta\beta\rangle + a_6|p_z\alpha\beta\rangle + a_7|p_+\alpha\beta\rangle + a_8|p_-\alpha\beta\rangle \\ & + a_9|p_z\beta\beta\rangle + a_{10}|p_+\beta\alpha\rangle + a_{11}|p_-\beta\alpha\rangle + a_{12}|p_z\alpha\alpha\rangle,\end{aligned} \tag{6}$$

where

$$|p_+\rangle = -\frac{1}{\sqrt{2}}|p_x + ip_y\rangle, \quad |p_-\rangle = \frac{1}{\sqrt{2}}|p_x - ip_y\rangle. \tag{7}$$

Here the former and latter α (β) are the valence-electron and conduction-electron up (down) spin functions, respectively. Using Eqs. (3) and (6), the valence-electron and conduction-electron matrix is obtained as shown in Table I.

The relative oscillator strengths in each direction can be obtained by considering the selection rules of the electric-dipole transitions, which are written as

$$\begin{aligned}&\text{for } x \text{ direction:} \frac{1}{2}|-a_1 + a_2 - a_4 + a_5|^2, \\ &\text{for } y \text{ direction:} \frac{1}{2}|a_1 + a_2 + a_4 + a_5|^2, \\ &\text{for } z \text{ direction:} |a_9 + a_{12}|^2.\end{aligned} \tag{8}$$

To obtain the oscillator strengths for arbitrary directions, we need to introduce new orthonormal coordinates of (x',y',z'). Figure 1 depicts the relationship between (x,y,z) and (x',y',z'). The oscillator strengths for arbitrary directions can be obtained by solving $UH^{\text{Wurtzite}}U^{-1}|\Psi'_{\text{exciton}}\rangle = E|\Psi'_{\text{exciton}}\rangle$, where U is the Unitary transformation operator and $|\Psi'_{\text{exciton}}\rangle$ is a new exciton wave function under the (x',y',z') coordinates. The definition of the Unitary transformation operator is given in Appendix.

When a uniaxial stress is introduced, the relationship between strain and stress tensors can be given by Hooke's law[35]

$$\begin{pmatrix}\epsilon_{xx}\\ \epsilon_{yy}\\ \epsilon_{zz}\\ 2\epsilon_{yz}\\ 2\epsilon_{zx}\\ 2\epsilon_{xy}\end{pmatrix} = \begin{pmatrix}s_{11} & s_{12} & s_{13} & 0 & 0 & 0\\ s_{12} & s_{11} & s_{13} & 0 & 0 & 0\\ s_{13} & s_{13} & s_{33} & 0 & 0 & 0\\ 0 & 0 & 0 & s_{44} & 0 & 0\\ 0 & 0 & 0 & 0 & s_{44} & 0\\ 0 & 0 & 0 & 0 & 0 & s_{66}\end{pmatrix} \begin{pmatrix} F'_{xx}\cos^2\theta + 2F'_{zx}\sin\theta\cos\theta + F'_{zz}\sin^2\theta \\ F'_{yy} \\ F'_{xx}\sin^2\theta - 2F'_{zx}\sin\theta\cos\theta + F'_{zz}\cos^2\theta \\ F'_{yz}\cos\theta - F'_{xy}\sin\theta \\ -F'_{xx}\sin\theta\cos\theta + F'_{zx}(\cos^2\theta - \sin^2\theta) + F'_{zz}\sin\theta\cos\theta \\ F'_{yz}\sin\theta + F'_{xy}\cos\theta \end{pmatrix}, \tag{9}$$

where s_{ij} and F_{ij} denote the elastic compliance constants and stress tensors, respectively.

GaN-related materials typically form a hexagonal structure in the wurtzite phase and have crystal symmetry belonging to the C_{6v} point group. As discussed in Ref. 36, the irreducible representation of the conduction band is Γ_7^C whereas those of the valence bands are Γ_9^V, Γ_7^V, and Γ_7^V. These conduction band and valence bands are doubly degenerated due to the spin. To consider the irreducible representations of excitons, direct products of those of the conduction band and the valence bands are needed. Figure 2 shows the irreducible representation of the band-to-band model and the exciton model. The irreducible representations of Γ_5 and Γ_1 are dipole allowed for $E \perp c$ and $E \| c$, respectively.

When uniaxial stress perpendicular to the c-plane is introduced, the crystal symmetry is reduced and the point group changes from C_{6v} to C_{2v}. Figure 3 illustrates the irreducible representations of the excitons. The irreducible representations of Γ_2, Γ_4, and Γ_1 are dipole allowed for $E \| x$, $E \| y$, and $E \| z$, respectively, where the x and y directions are no longer equivalent.

III. EXPERIMENTAL AND ASSIGNMENT

The samples used in this study were a-plane and $(11\bar{2}2)$ plane bulk GaN substrates grown by hydride vapor phase epitaxy (HVPE). Their surfaces were chemically and mechanically polished. Etch-pit density and residual carrier concentration were approximately 10^6 cm^{-2} and 10^{17} cm^{-3}, respectively. The samples were cut into a cuboid shape by a laser scriber and mechanically lapped until optically flat edges were obtained. Typical dimensions of these cuboid samples were $3 \times 3 \times 0.5$ mm^3.

A uniaxial stress-loading system operating at cryogenic temperature was constructed. Polarized reflectance spectroscopy under uniaxial stress was performed using a Xe-lamp and a Glan-Taylor polarizer combined with this system. The signals were dispersed by a 1-m monochromator (1200 grooves/mm) and detected by a photomultiplier tube employing conventional lock-in techniques. The current experimental setup had a resolution of approximately 0.01 nm. When we transformed the wavelengths into energies, a refractive index of air, n_{air}=1.000277 was used. All experiments were performed at the normal incidence condition at nearly 4.2 K.

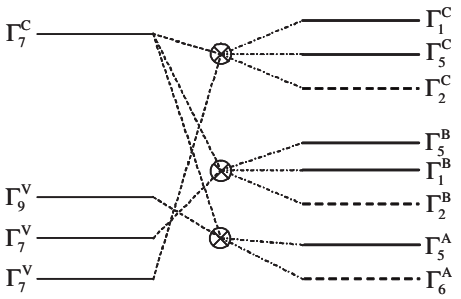

FIG. 2. Irreducible representations of the band-to-band model and exciton model in the C_{6v} point group. The arrangement in the exciton model was determined by our experiments. Broken lines are dipole forbidden.

To confirm the operation of the uniaxial stress-loading system, we performed polarized reflectance measurements on *c*-plane GaN films grown on sapphire substrates. Uniaxial stress was applied perpendicular to the *a*-plane, which is the same condition reported in Ref. 30. It was confirmed that the uniaxial stress-loading system worked properly because our data and that in Ref. 30 quantitatively agree (data not shown).

Before describing the experimental results, the role of the exciton deformation potentials (C_1–C_6) in determining the electronic structures is explained. If the crystal symmetry belongs to the C_{6v} point group, ϵ_{xx} and ϵ_{yy} are equivalent and all the nondiagonal terms of the strain tensors are zero. Therefore, the uniaxial stress dependence of the energy difference between exciton transitions (relative exciton-transition energies) are determined by only the exciton deformation potentials of C_3 and C_4. When the crystal symmetry is reduced from the C_{6v} to the C_{2v} point group, the exciton deformation potential of C_5 as well as C_3 and C_4 are necessary to describe the uniaxial stress dependence of the relative exciton-transition energies because the strain tensors of ϵ_{xx} and ϵ_{yy} are no longer equivalent. In addition, applying stress along an off-crystal axis direction further reduces the crystal symmetry, when the exciton deformation potential of C_6 is also necessary to describe the uniaxial stress dependence of the relative exciton-transition energies. The exciton deformation potentials of C_1 and C_2 are only required to explain the uniaxial stress dependence of the absolute exciton-transition energies.

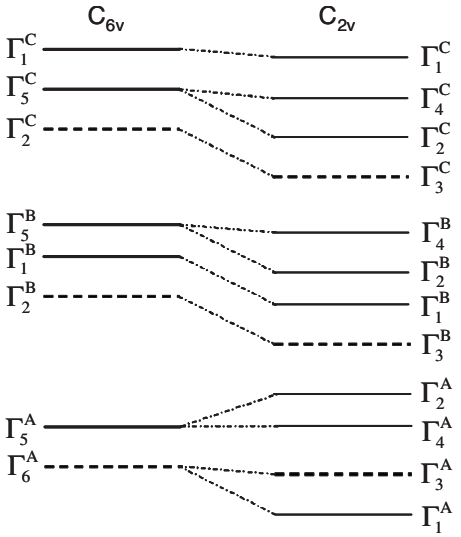

FIG. 3. Symmetry breaking from the point group of C_{6v}–C_{2v}. Broken lines are dipole forbidden.

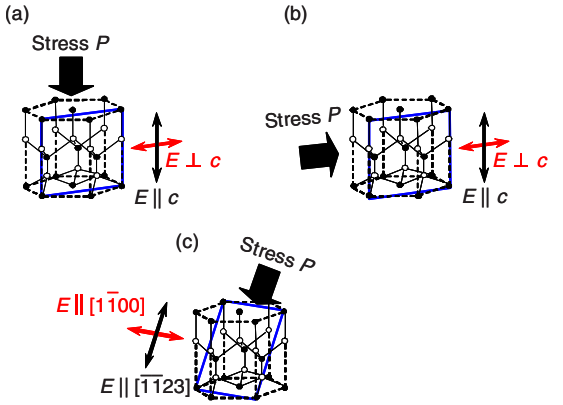

FIG. 4. (Color online) Experimental configurations (a) $P \| c$, (b) $P \perp c$, and (c) $P \| [\bar{1}\bar{1}23]$.

Initially, polarized reflectance measurements were performed on the *a*-plane bulk GaN substrate under uniaxial stress perpendicular to the *c*-plane ($P \| c$). Figures 4(a) and 5 show the configuration and results, respectively. The uniaxial stress dependence of some reflection anomalies with sharp linewidths were observed for both $E \| c$ and $E \perp c$. Using group theory on excitons as discussed above, the resonances observed for $E \| c$ were assigned to $\Gamma_1^B(n=1)$, $\Gamma_1^C(n=1)$, and $\Gamma_1^C(n=2)$ on the order of the photon energy. As the uniaxial stress increased, a new anomaly appeared nearby $\Gamma_1^C(n=1)$, which we assigned to $\Gamma_1^B(n=2)$ considering the stress dependence and exciton binding energy. Likewise, the resonances observed for $E \perp c$ were assigned to $\Gamma_5^A(n=1)$, $\Gamma_5^B(n=1)$, $\Gamma_5^A(n=2)$, and $\Gamma_5^C(n=1)$. It should be noted that a weak feature was also observed on the lower energy side of $\Gamma_5^A(n$

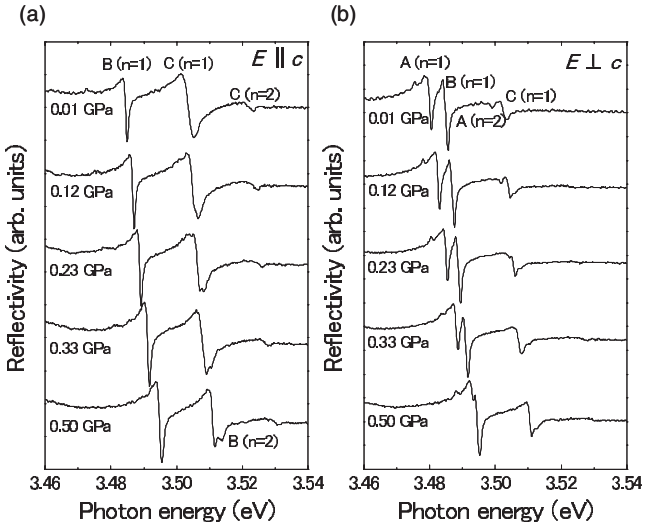

FIG. 5. Reflectance spectra of the *a*-plane GaN bulk substrate under uniaxial stress $P \| c$. (a) $E \| c$ and (b) $E \perp c$.

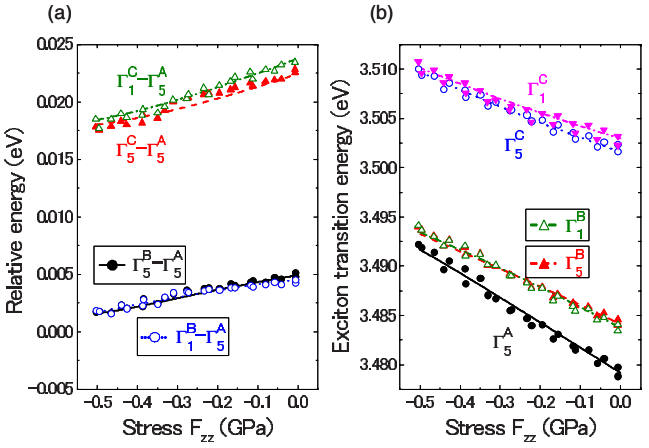

FIG. 6. (Color online) Uniaxial stress dependence of exciton-transition energies for $P\|c$. (a) Relative to $\Gamma_5^A(n=1)$ and (b) absolute values. Symbols represent the experimental data whereas the lines are the fitted results.

$=1$) and we assigned it to an impurity-related exciton of $\Gamma_5^A(n=1)$ considering the uniaxial stress dependence. Since we mainly focus on the intrinsic optical properties of GaN in this paper, these features are neglected in the following discussions.

Here, we assumed that the exciton-transition energies correspond to the average energies between those for the reflection maxima and the minima. The exciton-transition energies obtained in this analysis agreed well with those extracted by the fitting based on the exciton-transition model.[37] It should be noted that reflectance spectra should be interpreted by the exciton-polariton model, which includes spatial dispersion.[38,39] However, it has been reported that the fitting results using the exciton-transition model and the exciton-polariton model are within the experimental error for GaN,[40] which is why we neglected the exciton-polariton effects in this study. Figure 6 shows the uniaxial stress dependence of the relative energies with respect to $\Gamma_5^A(n=1)$ and the absolute exciton-transition energies.

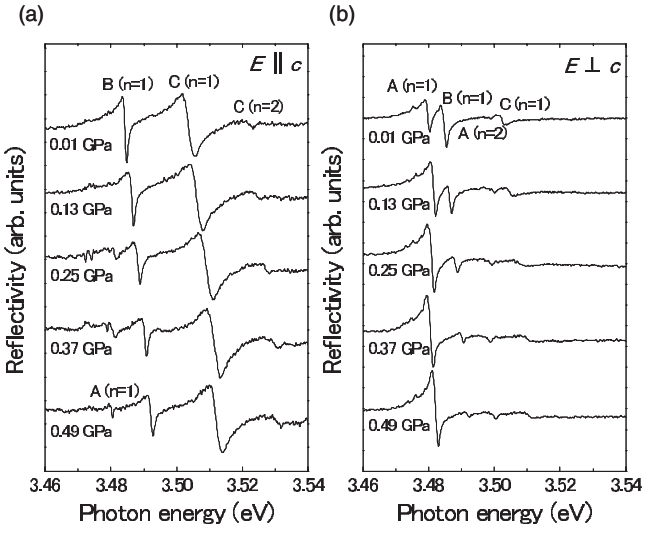

FIG. 7. Reflectance spectra of the a-plane GaN bulk substrate under uniaxial stress $P\perp c$. (a) $E\|c$ and (b) $E\perp c$.

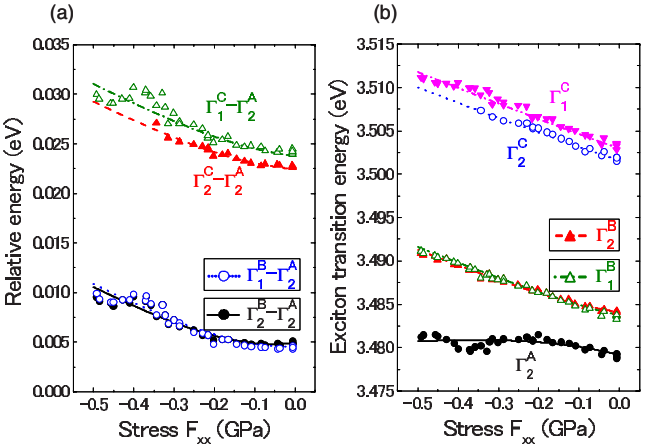

FIG. 8. (Color online) Uniaxial stress dependence of exciton-transition energies for $P\perp c$. (a) Relative to $\Gamma_2^A(n=1)$ and (b) absolute values. Symbols represent experimental data whereas the lines are the fitted results.

Secondary, polarized reflectance measurements were performed on the a-plane bulk GaN substrate under uniaxial stress perpendicular to the m-plane ($P\perp c$). Figures 4(b) and 7 show the configuration and results, respectively. Using group theory on excitons, the resonances observed for $E\|c$ were assigned to $\Gamma_1^B(n=1)$, $\Gamma_1^C(n=1)$, and $\Gamma_1^C(n=2)$ on the order of photon energy. Under high stress, a new feature, which was assigned to $\Gamma_1^A(n=1)$ by considering group theory, appeared around 3.480 eV. Similarly, the resonances observed for $E\perp c$ were assigned to $\Gamma_2^A(n=1)$, $\Gamma_2^B(n=1)$, $\Gamma_2^A(n=2)$, and $\Gamma_2^C(n=1)$. Figure 8 shows the uniaxial stress dependence of the relative energies with respect to $\Gamma_2^A(n=1)$ and the absolute exciton-transition energies.

Finally, we performed polarized reflectance measurements on the $(11\bar{2}2)$ plane bulk GaN substrate under uniaxial stress $P\|[\bar{1}\bar{1}23]$. Figures 4(c) and 9 show the configuration and

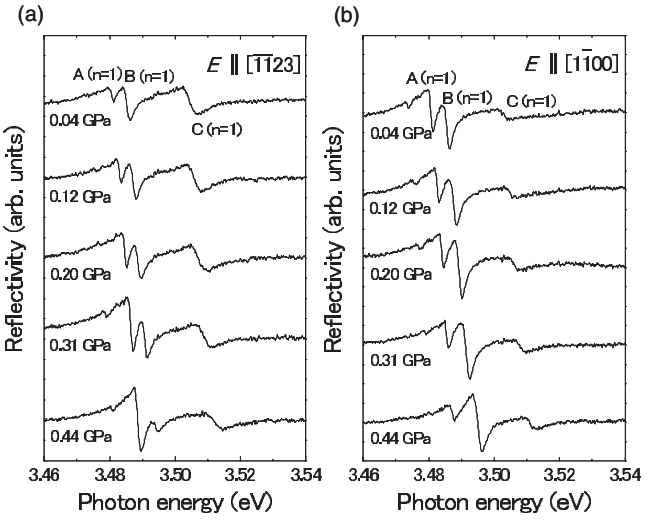

FIG. 9. Reflectance spectra of the $(11\bar{2}2)$ plane GaN bulk substrate under uniaxial stress $P\|[\bar{1}\bar{1}23]$. (a) $E\|[\bar{1}\bar{1}23]$ and (b) $E\|[1\bar{1}00]$.

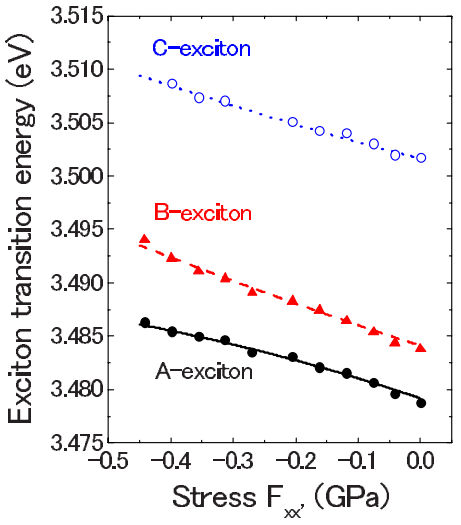

FIG. 10. (Color online) Uniaxial stress dependence of exciton-transition energies on the $(11\bar{2}2)$ plane GaN bulk substrates $P\|[\bar{1}\bar{1}23]$ and $E\|[1\bar{1}00]$. Symbols represent experimental data whereas the lines are the fitted results.

results, respectively. So far, C_6 has not been experimentally determined but it has been obtained by the quasicubic approximation. In contrast, the current configuration enables the exciton deformation potential of C_6 to be experimentally determined because shear strain is induced. For $E\|[\bar{1}\bar{1}23]$, three exciton transitions were resolved as shown in Fig. 9(a) although six exciton transitions are theoretically dipole allowed. This is because three of six exciton transitions with relatively large oscillator strengths were experimentally observed for $E\|[\bar{1}\bar{1}23]$. This situation may cause misassignment on excitons. On the other hand, in the case of $E\|[1\bar{1}00]$, we experimentally observed three exciton transitions as shown in Fig. 9(b) and found that three exciton transitions are theoretically dipole allowed. Therefore, we assigned the exciton-transition energies only for this configuration. Figure 10 shows the uniaxial stress dependence of the absolute exciton-transition energies.

IV. DISCUSSION

Initially, the experimental results for samples under no stress were analyzed in order to obtain the "bulk parameters:" Δ_1, Δ_2, Δ_3, and j. In this particular case, the exciton-transition energies were deduced by the exciton-model fitting. The bulk parameters were completely determined from the relative exciton-transition energies. We assumed that our samples were strain free. Table II lists the bulk parameters and the relative exciton-transition energies. Δ_2 and Δ_3 agree well with the reported values but Δ_1 appears somewhat larger. Reference 23 has noted that the residual strain in HVPE samples may cause an overestimation of Δ_1. However, if the short-range Coulomb interaction is not considered, deduction from the relative exciton-transition energies of $\Gamma_5^B-\Gamma_5^A$ and $\Gamma_5^C-\Gamma_5^A$ indicate that $\Delta_1=9.8$ meV, $\Delta_2=5.9$ meV, and $\Delta_3=6.0$ meV. These values are in excellent agreement with those of a homoepitaxial GaN.[37] Therefore, we believe that Δ_1 is larger due to the short-range Coulomb interaction rather than the residual biaxial strain. Hence, the short-range Coulomb interaction is important in determining the bulk parameters. Next, we examined the value of j. To date, j has been experimentally extracted by the relative exciton-transition energy between Γ_5^B and Γ_1^B. However, as shown in Fig. 11, it should be determined by the relative exciton-transition energy between Γ_5^C and Γ_1^C rather than between Γ_5^B and Γ_1^B. Hence, we simultaneously performed the least-squares fitting for all observables and determined the bulk parameters in GaN. Table II shows the results.

Next, the uniaxial stress dependence of the exciton-transition energies was analyzed using the analytical expressions of the valence-electron and conduction-electron matrix derived by Gil *et al.*[22,41] due to their usefulness in the least-squares fitting. When a uniaxial stress is applied perpendicular to the c-plane ($P\|c$), the relative exciton-transition ener-

TABLE II. Relative exciton-transition energies and bulk parameters in units of meV. Relative exciton-transition energies are calculated by bulk parameters.

Experimental	$\Gamma_5^B-\Gamma_5^A$	$\Gamma_5^C-\Gamma_5^A$	$\Gamma_1^B-\Gamma_5^A$	$\Gamma_1^C-\Gamma_5^A$	Δ_1	Δ_2	Δ_3	j
Korona *et al.*[a]	5.1	23.9	5.1	23.9	9.3	6.6	6.6	
Yamaguchi *et al.*[b]	4.5	22.0	4.5	22.0	10.0	5.5	6.0	
Shikanai *et al.*[c]	7.4	29.6	7.4	29.6	22.0	5.0	5.0	
Gil *et al.*[d]	4.3	21.2	3.7	23.1	10.0	5.1	6.1	2.0
Gil *et al.*[e]	4.3	21.1	4.4	21.5	8.7	5.7	5.9	0.6
Paskov *et al.*[f]	6.1	22.0	6.2	22.5	10.0	6.2	5.5	0.6
Paskov *et al.*[f]	4.4	21.7	4.4	22.2	10.0	5.5	6.0	0.6
Present work	4.9	22.5	4.6	23.8	12.3	5.2	5.9	1.2

[a]Reference. 37.
[b]Reference. 23.
[c]Reference. 21.
[d]Reference. 41.
[e]Reference. 42.
[f]Reference. 43.

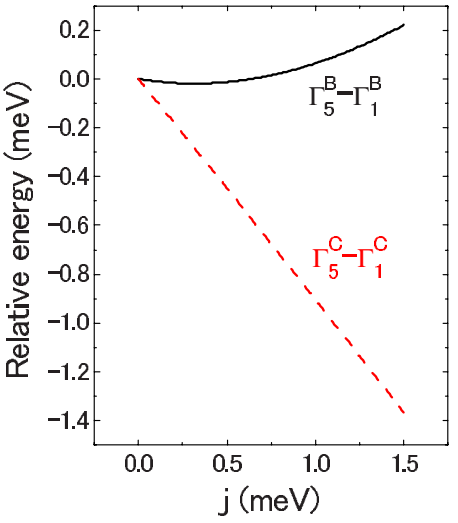

FIG. 11. (Color online) Relative energies are plotted as a function of the spin-exchange interaction coefficient. Calculation parameters are $\Delta_1=10.0$ meV, $\Delta_2=5.5$ meV, and $\Delta_3=6.0$ meV (Ref. 43).

gies are completely determined by the parameter α^μ as follows:

$$\alpha^\mu = C_3S_{33} + 2C_4S_{13}. \tag{10}$$

We performed the least-squares fitting for all the observables and obtained $\alpha^\mu=0.0174$ eV/GPa.

Likewise, when a uniaxial stress is introduced perpendicular to the m-plane ($P\perp c$), the relative exciton-transition energies can be determined by the following two parameters:

$$\beta^\mu = C_3S_{13} + C_4(S_{11}+S_{12}),$$

$$\beta^a = -C_5(S_{11}-S_{12}). \tag{11}$$

Using the same procedure, we obtained $\beta^\mu=-0.0136$ eV/GPa and $\beta^a=0.0116$ eV/GPa.

Also, for the $(11\bar{2}2)$ plane with $P\|[\bar{1}\bar{1}23]$, the following three parameters are necessary:

$$\gamma^\mu = C_3(S_{13}\cos^2\theta + S_{33}\sin^2\theta) + C_4[(S_{11}+S_{12})\cos^2\theta + 2S_{13}\sin^2\theta],$$

$$\gamma^a = -C_5(S_{11}-S_{12})\cos^2\theta,$$

$$\gamma^s = \frac{1}{2}C_6S_{44}\sin\theta\cos\theta. \tag{12}$$

The least-squares fitting gave $\gamma^\mu=0.0086$ eV/GPa, $\gamma^a=0.0026$ eV/GPa, and $\gamma^s=-0.0081$ eV/GPa. At this stage, α, β, and γ were determined separately from their respective experiments.

Then, to obtain the exciton deformation potentials from Eqs. (10)–(12), the values of the elastic constants must be determined. Although numerous sets of the elastic constants have been proposed using both first-principles calculations and experiments such as brillouin scattering or resonance ultrasound method,[44] the values are largely scattered. Herein,

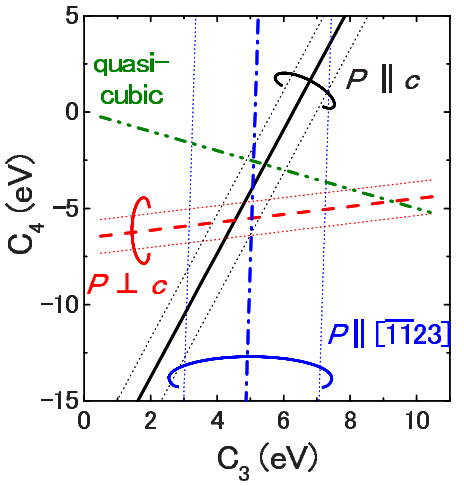

FIG. 12. (Color online) Relations between C_3 and C_4 obtained by experiments under three different conditions, $P\|c$, $P\perp c$, and $P\|[\bar{1}\bar{1}23]$ are plotted. Dotted lines represent experimental errors.

we chose the elastic constants proposed by Yamaguchi *et al.*[45] because this study determined the elastic constants using bulk GaN substrates. It should be noted that the elastic constants in GaN were assumed to be independent of temperature.[46]

With the selected set of elastic constants, we obtained three equations for the relationship between C_3 and C_4 (α^μ, β^μ, and γ^μ), two equations for C_5 (β^a and γ^a), and one equation for $C_6(\gamma^s)$. To extract the most plausible four parameters (C_3 to C_6) from these six equations, C_3 and C_4 were initially determined because these were experimental observables in all the experiments. Figure 12 plots the three relations between C_3 and C_4 using the elastic constants in Ref. 45. These three relations form a triangle and selecting the position close to the center simultaneously minimizes the errors in all the experiments. Thus, the values for C_3 and C_4 were 4.9 and −5.0 eV, respectively.

Next, β^a, γ^a, and γ^s were re-evaluated using the least-squares fitting where β^μ and γ^μ were constants using the above values of C_3 and C_4. Consequently, $C_5=-2.8$ eV and $C_6=-3.1$ eV were obtained. To determine the sign of C_5 and C_6, the uniaxial stress dependence of the oscillator strengths as well as the exciton-transition energies were considered.

Finally, C_1 and C_2 were determined from the absolute exciton-transition energies. Similar to C_3, and C_4, C_1 and C_2 were experimental observables in all the experiments. Therefore, the same procedure was used to evaluate C_1 and C_2 as 6.5 and 11.2 eV, respectively.

Using the exciton deformation potentials obtained by the current analysis, theoretical calculations were performed and the results are shown in Figs. 6, 8, and 10. The accuracies of the exciton deformation potentials of $C_{i=1,2,3,4,5}$ and C_6 were about 10% and 20%, respectively. It must be emphasized that the experimental uniaxial stress dependence of the exciton oscillator strengths can also be qualitatively described by theoretical calculations using our values. Table III lists the exciton deformation potentials. If the elastic constants proposed by Polian *et al.*[56] were used then the exciton-deformation potentials were $C_1=7.6$ eV, $C_2=11.8$ eV, C_3

TABLE III. Exciton deformation potentials in GaN and other wurtzite II-VI compounds.

GaN (experimental)	C_1	C_2	C_3	C_4	C_5	C_6	$C_3/(-2C_4)$
Shan *et al.*[a]	6.5	11.8	5.3	−2.7			0.98
Shikanai *et al.*[b]			8.82	−4.41			1
Peng *et al.*[c]	9.6	8.2	1.9	−1.0			0.95
Gil *et al.*[d]	6.85	8.84	1.99	−1.0			1
Alemu *et al.*[e]	5.32	10.23	4.91	−2.50	−2.4		0.98
Yamaguchi *et al.*[f]			6.8	−3.4	−3.3		1
Ghosh *et al.*[g]	3.1	11.2	8.2	−4.1	−4.7		1
Vurgaftman *et al.*[h]	4.9	11.3	8.2	−4.1	−4.0	(−5.5)	1
Vurgaftman *et al.*[i]	7.1	9.9	5.2	−2.7	−2.8	(−4.3)	0.96
Chuang *et al.*[j]	4.78	6.18	1.4	−0.7			1
Present work	6.5	11.2	4.9	−5.0	−2.8	−3.1	0.49
GaN (calculation)							
Ohtoshi *et al.*[k]			6.6	−3.3	−4.0		1
Suzuki *et al.*[l]			2.99	−1.50	−2.04	−3.67	1
Kumagai *et al.*[m]	2.9	10.9	8.0	−4.0			1
Wagner *et al.*[n]	4.09	8.87	7.02	−3.65			0.96
Yan *et al.*[o]	5.81	8.92	5.47	−2.98	−2.82		0.92
Shimada *et al.*[p]			5.80	−3.25	−2.85		0.89
Majewski *et al.*[q]			6.61	−3.55			0.93
Kim *et al.*[r]			5.7	−2.85			1
II-VI compounds (experimental)							
ZnO[s]	3.8	3.8	0.8	−1.4	−1.2	|1.0|	0.29
ZnO[t]	3.90	4.13	1.15	−1.22	−1.53	−0.92	0.47
CdS[s]	2.8	4.5	1.3	−2.9	−1.5	|1.2|	0.22
CdSe[s]	0.76	3.7	4.0	−2.2	1.2	|1.5|	0.91

[a]Reference. 20.
[b]Reference. 21.
[c]Reference. 47.
[d]Reference. 22.
[e]Reference. 24.
[f]Reference. 30.
[g]Reference. 25.
[h]Reference. 44 C_6 is not observable (quasicubic approximation).
[i]Reference. 48 C_6 is not observable (quasicubic approximation).
[j]Reference. 32.
[k]Reference. 49.
[l]Reference. 12.
[m]Reference. 50.
[n]Reference. 51.
[o]Reference. 52.
[p]Reference. 53.
[q]Reference. 54.
[r]Reference. 55.
[s]Reference. 28.
[t]Reference. 29.

=4.5 eV, C_4=−4.8 eV, C_5=−2.9 eV, and C_6=−3.6 eV.

It is found that our exciton deformation potentials significantly differ from previous studies, especially the relation between C_3 and C_4. The well-known approximation in the hexagonal symmetry, that is, the quasicubic approximation, can be written as

$$D_1 - D_2 = -D_3 = 2D_4, \quad D_3 + 4D_5 = \sqrt{2}D_6. \tag{13}$$

Using our notation, Eq. (13) can be written as

$$C_1 - C_2 - (a_{cz} - a_{ct}) = -C_3 = 2C_4,$$

$$C_3 + 4C_5 = \sqrt{2}C_6. \tag{14}$$

To explain the quasicubic approximation in hexagonal wurtzite structures, the ideal sp^3 tetrahedral bond configuration in cubic zincblende structures must be recalled. In "ideal" hexagonal wurtzite structures, the ideal sp^3 tetrahedron is preserved, and c/a must equal 1.63299,[57] when the quasicubic approximation is strictly applicable. However, if the c/a ratio deviates from the ideal value, the quasicubic approximation need not to be rigorously satisfied.

To date, the quasicubic approximation has been considered a good approximation in GaN which has a c/a ratio of

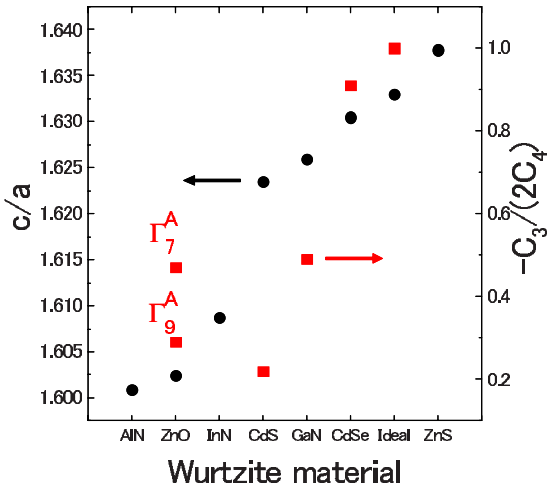

FIG. 13. (Color online) Ratio of c/a and $-C_3/2C_4$ for select wurtzite compounds.

1.6259. Gil and co-workers[58] have suggested that this approximation is experimentally supported because significant differences between the hydrostatic stress dependence of heavy hole and other bands in the absorption spectra are not present. In fact, $C_3=-2C_4$ must be satisfied as long as the hydrostatic strain does not vary the energy difference between the heavy-hole band and the other bands. However, the absorption spectra[59,60] that Gil *et al.* relied on do not exhibit clear exciton-related transitions and the relation between C_3 and C_4 is generally different between under hydrostatic stress and hydrostatic strain. Thus, their assertion does not seem firm.

Table III also lists the deformation potentials in II-VI compounds. It should be noted that the valence-band ordering of ZnO is still controversial.[61,62] Langer *et al.*[28] have reported that the irreducible representation of the topmost valence band is Γ_9^A, while Wrzesinski and Fröohlich[29] have assigned that the valence-band ordering is Γ_7^A-Γ_9^B-Γ_7^C. The different assignment of the valence bands may cause the differences between the deformation potentials in ZnO in Refs. 28 and 29. Because it cannot be concluded which arrangement is correct at this stage, both the deformation potentials are listed in Table III. Herein, we evaluated the deviation from the quasicubic approximation by comparing $C_3/(-2C_4)$. The deformation potentials in ZnO and CdS do not satisfy the quasicubic approximation most likely because they have "nonideal" wurtzite structures. Figure 13 plots the c/a ratio for select wurtzite semiconductors. It is found that the deviation from the quasicubic approximation is correlated with the c/a ratio. Therefore, we concluded that our exciton deformation potentials in GaN show the breakdown of the quasicubic approximation.

V. CONCLUSION

Reflectance spectroscopy for nonpolar and semipolar bulk GaN substrates under uniaxial stress was performed. Bir-Pikus theory was expanded to describe the optical properties of wurtzite materials grown on semipolar planes, where the short-range Coulomb interaction was considered. Fitting the experimental results with calculations provided all the exciton deformation potentials as $C_1=6.5$ eV, $C_2=11.2$ eV, $C_3=4.9$ eV, $C_4=-5.0$ eV, $C_5=-2.8$ eV, and $C_6=-3.1$ eV as well as bulk parameters. The obtained values clearly indicate a breakdown of the quasicubic approximation in GaN.

ACKNOWLEDGMENTS

This research was partially supported by the Ministry of Education, Culture, Sports, Science, and Technology of Japan, Grant-in-Aid for Scientific Research on Priority Areas, under Grant No. 21016006.

APPENDIX: DERIVATION OF THE UNITARY TRANSFORMATION MATRIX

In this appendix, the unitary transformation matrix, which is used to obtain oscillator strengths for arbitrary directions, is derived. In the (x,y,z) orthonormal coordinates, the Schrödinger equation can be written as

$$H^{\text{Wurtzite}}|\Psi^{\text{exciton}}\rangle = E|\Psi^{\text{exciton}}\rangle. \tag{A1}$$

Here, we introduce an exciton wave function as $|\Psi^{\text{exciton}}\rangle' = U|\Psi^{\text{exciton}}\rangle$, where U is the unitary transformation matrix. $|\Psi^{\text{exciton}}\rangle'$ is defined as

$$\begin{aligned}|\Psi^{\text{exciton}}\rangle' = {} & a_1|p_{+'}\alpha\alpha\rangle + a_2|p_{-'}\alpha\alpha\rangle + a_3|p_{z'}\beta\alpha\rangle + a_4|p_{+'}\beta\beta\rangle + a_5|p_{-'}\beta\beta\rangle + a_6|p_{z'}\alpha\beta\rangle \\ & + a_7|p_{+'}\alpha\beta\rangle + a_8|p_{-'}\alpha\beta\rangle + a_9|p_{z'}\beta\beta\rangle + a_{10}|p_{+'}\beta\alpha\rangle + a_{11}|p_{-'}\beta\alpha\rangle + a_{12}|p_{z'}\alpha\alpha\rangle,\end{aligned} \tag{A2}$$

where

$$|p_{+'}\rangle = -\frac{1}{\sqrt{2}}|p_{x'} + ip_{y'}\rangle, \quad |p_{-'}\rangle = \frac{1}{\sqrt{2}}|p_{x'} - ip_{y'}\rangle. \tag{A3}$$

Equation (A1) can be rewritten under the (x',y',z') coordinates as

$$UH^{\text{Wurtzite}}U^{-1}|\Psi'_{\text{exciton}}\rangle = E|\Psi'_{\text{exciton}}\rangle. \tag{A4}$$

The unitary transformation matrix U can be derived considering the coordinate transformation from (x,y,z) to (x',y',z') to give the following matrix:

$$U=\begin{pmatrix}
\frac{(1+\cos\theta)}{2} & \frac{(1-\cos\theta)}{2} & 0 & 0 & 0 & 0 & 0 & 0 & 0 & 0 & 0 & \frac{\sin\theta}{\sqrt{2}} \\
\frac{(1-\cos\theta)}{2} & \frac{(1+\cos\theta)}{2} & 0 & 0 & 0 & 0 & 0 & 0 & 0 & 0 & 0 & -\frac{\sin\theta}{\sqrt{2}} \\
0 & 0 & \cos\theta & 0 & 0 & 0 & 0 & 0 & 0 & -\frac{\sin\theta}{\sqrt{2}} & \frac{\sin\theta}{\sqrt{2}} & 0 \\
0 & 0 & 0 & \frac{(1+\cos\theta)}{2} & \frac{(1-\cos\theta)}{2} & 0 & 0 & 0 & \frac{\sin\theta}{\sqrt{2}} & 0 & 0 & 0 \\
0 & 0 & 0 & \frac{(1-\cos\theta)}{2} & \frac{(1+\cos\theta)}{2} & 0 & 0 & 0 & -\frac{\sin\theta}{\sqrt{2}} & 0 & 0 & 0 \\
0 & 0 & 0 & 0 & 0 & \cos\theta & -\frac{\sin\theta}{\sqrt{2}} & \frac{\sin\theta}{\sqrt{2}} & 0 & 0 & 0 & 0 \\
0 & 0 & 0 & 0 & 0 & \frac{\sin\theta}{\sqrt{2}} & \frac{(1+\cos\theta)}{2} & \frac{(1-\cos\theta)}{2} & 0 & 0 & 0 & 0 \\
0 & 0 & 0 & 0 & 0 & -\frac{\sin\theta}{\sqrt{2}} & \frac{(1-\cos\theta)}{2} & \frac{(1+\cos\theta)}{2} & 0 & 0 & 0 & 0 \\
0 & 0 & 0 & -\frac{\sin\theta}{\sqrt{2}} & \frac{\sin\theta}{\sqrt{2}} & 0 & 0 & 0 & \cos\theta & 0 & 0 & 0 \\
0 & 0 & \frac{\sin\theta}{\sqrt{2}} & 0 & 0 & 0 & 0 & 0 & 0 & \frac{(1+\cos\theta)}{2} & \frac{(1-\cos\theta)}{2} & 0 \\
0 & 0 & -\frac{\sin\theta}{\sqrt{2}} & 0 & 0 & 0 & 0 & 0 & 0 & \frac{(1-\cos\theta)}{2} & \frac{(1+\cos\theta)}{2} & 0 \\
-\frac{\sin\theta}{\sqrt{2}} & \frac{\sin\theta}{\sqrt{2}} & 0 & 0 & 0 & 0 & 0 & 0 & 0 & 0 & 0 & \cos\theta
\end{pmatrix}.$$

*ryota.ishii@optomater.kuee.kyoto-u.ac.jp
†kawakami@kuee.kyoto-u.ac.jp

[1] S. Nakamura and G. Fasol, *The Blue Laser Diode* (Springer-Verlag, Berlin, 1997).
[2] Y. Narukawa, M. Sano, T. Sakamoto, T. Yamada, and T. Mukai, Phys. Status Solidi A **205**, 1081 (2008).
[3] S. H. Park and S. L. Chuang, Phys. Rev. B **59**, 4725 (1999).
[4] T. Takeuchi, H. Amano, and I. Akasaki, Jpn. J. Appl. Phys. **39**, 413 (2000).
[5] P. Waltereit, O. Brandt, A. Trampert, H. T. Grahn, J. Menniger, M. Ramsteiner, M. Reiche, and K. H. Ploog, Nature (London) **406**, 865 (2000).
[6] K. Nishizuka, M. Funato, Y. Kawakami, Sg. Fujita, Y. Narukawa, and T. Mukai, Appl. Phys. Lett. **85**, 3122 (2004).
[7] M. Funato, M. Ueda, Y. Kawakami, Y. Narukawa, T. Kosugi, M. Takahashi, and T. Mukai, Jpn. J. Appl. Phys., Part 2 **45**, L659 (2006).
[8] M. Kubota, K. Okamoto, T. Tanaka, and H. Ohta, Appl. Phys. Express **1**, 011102 (2008).
[9] Y. Tsuda, M. Ohta, P. O. Vaccaro, S. Ito, S. Hirukawa, Y. Kawaguchi, Y. Fujishiro, Y. Takahira, Y. Ueta, T. Takakura, and T. Yuasa, Appl. Phys. Express **1**, 011104 (2008).
[10] A. Tyagi, H. Zhong, N. N. Fellows, M. Iza, J. S. Speck, S. P. DenBaars, and S. Nakamura, Jpn. J. Appl. Phys., Part 2 **46**, L129 (2007).
[11] Y. Yoshizumi, M. Adachi, Y. Enya, T. Kyono, S. Tokuyama, T. Sumitomo, K. Akita, T. Ikegami, M. Ueno, K. Katayama, and T. Nakamura, Appl. Phys. Express **2**, 092101 (2009).
[12] M. Suzuki and T. Uenoyama, J. Appl. Phys. **80**, 6868 (1996).
[13] A. A. Yamaguchi, Jpn. J. Appl. Phys., Part 2 **46**, L789 (2007).
[14] A. A. Yamaguchi, Appl. Phys. Lett. **94**, 201104 (2009).
[15] A. A. Yamaguchi, Phys. Status Solidi C **5**, 2329 (2008).
[16] M. Ueda, M. Funato, K. Kojima, Y. Kawakami, Y. Narukawa, and T. Mukai, Phys. Rev. B **78**, 233303 (2008).
[17] W. H. Kleiner and L. M. Roth, Phys. Rev. Lett. **2**, 334 (1959).
[18] G. L. Bir and G. E. Pikus, *Symmetry and Strain-Induced Effects in Semiconductors* (Wiley, New York, 1974).
[19] B. Gil, O. Briot, and R. L. Aulombard, Phys. Rev. B **52**, R17028 (1995).
[20] W. Shan, R. J. Hauenstein, A. J. Fischer, J. J. Song, W. G. Perry, M. D. Bremser, R. F. Davis, and B. Goldenberg, Phys. Rev. B **54**, 13460 (1996).
[21] A. Shikanai, T. Azuhata, T. Sota, S. F. Chichibu, A. Kuramata, K. Horino, and S. Nakamura, J. Appl. Phys. **81**, 417 (1997).
[22] B. Gil and A. Alemu, Phys. Rev. B **56**, 12446 (1997). Misprints in the matrix for Γ_2 were corrected in this paper.
[23] A. A. Yamaguchi, Y. Mochizuki, H. Sunakawa, and A. Usui, J. Appl. Phys. **83**, 4542 (1998).
[24] A. Alemu, B. Gil, M. Julier, and S. Nakamura, Phys. Rev. B **57**, 3761 (1998).
[25] S. Ghosh, P. Waltereit, O. Brandt, H. T. Grahn, and K. H. Ploog, Phys. Rev. B **65**, 075202 (2002).
[26] T. Koda and D. W. Langer, Phys. Rev. Lett. **20**, 50 (1968).
[27] F. H. Pollak and M. Cardona, Phys. Rev. **172**, 816 (1968).
[28] D. W. Langer, R. N. Euwema, K. Era, and T. Koda, Phys. Rev. B **2**, 4005 (1970).
[29] J. Wrzesinski and D. Fröhlich, Phys. Rev. B **56**, 13087 (1997).
[30] A. A. Yamaguchi, Y. Mochizuki, C. Sasaoka, A. Kimura, M. Nido, and A. Usui, Appl. Phys. Lett. **71**, 374 (1997).
[31] G. D. Mahan and J. J. Hopfield, Phys. Rev. **135**, A428 (1964).
[32] S. L. Chuang and C. S. Chang, Phys. Rev. B **54**, 2491 (1996).
[33] O. Akimoto and H. Hasegawa, Phys. Rev. Lett. **20**, 916 (1968).
[34] J. E. Rowe, M. Cardona, and F. H. Pollak, Solid State Commun. **6**, 239 (1968).
[35] J. F. Nye, *Physical Properties of Crystals* (Oxford University Press, NewYork, 1957).
[36] G. F. Koster, J. O. Dimmock, R. G. Wheeler, and H. Statz, *Properties of Thirty-Two Point Groups* (MIT Press, Cambridge, Massachusetts, 1963).
[37] K. P. Korona, A. Wysmolek, K. Pakula, R. Stepniewski, J. M.

Baranowski, I. Grzegory, B. Lucznik, M. Wroblewski, and S. Porowski, Appl. Phys. Lett. **69**, 788 (1996).
[38] J. J. Hopfield, Phys. Rev. **112**, 1555 (1958).
[39] K. Torii, T. Deguchi, T. Sota, K. Suzuki, S. Chichibu, and S. Nakamura, Phys. Rev. B **60**, 4723 (1999).
[40] K. Kornitzer, T. Ebner, K. Thonke, R. Sauer, C. Kirchner, V. Schwegler, M. Kamp, M. Leszczynski, I. Grzegory, and S. Porowski, Phys. Rev. B **60**, 1471 (1999).
[41] B. Gil and O. Briot, Phys. Rev. B **55**, 2530 (1997).
[42] M. Julier, J. Campo, B. Gil, J. P. Lascaray, and S. Nakamura, Phys. Rev. B **57**, R6791 (1998).
[43] P. P. Paskov, T. Paskova, P. O. Holtz, and B. Monemar, Phys. Rev. B **64**, 115201 (2001).
[44] I. Vurgaftman and J. R. Meyer, J. Appl. Phys. **94**, 3675 (2003).
[45] M. Yamaguchi, T. Yagi, T. Sota, T. Deguchi, K. Shimada, and S. Nakamura, J. Appl. Phys. **85**, 8502 (1999).
[46] R. R. Reeber and K. Wang, MRS Internet J. Nitride Semicond. Res. **6**, 3 (2001).
[47] H. Y. Peng, M. D. McCluskey, Y. M. Gupta, M. Kneissl, and N. M. Johnson, Phys. Rev. B **71**, 115207 (2005).
[48] I. Vurgaftman and J.R. Meyer, in *Nitride Semiconductor Devices: Principles and Simulations*, edited by J. Piprek(Wiley-VCH, New York, 2007), Chap. 2.
[49] T. Ohtoshi, A. Niwa, and T. Kuroda, J. Appl. Phys. **82**, 1518 (1997).
[50] M. Kumagai, S. L. Chuang, and H. Ando, Phys. Rev. B **57**, 15303 (1998).
[51] J. M. Wagner and F. Bechstedt, Phys. Rev. B **66**, 115202 (2002).
[52] Q. Yan, P. Rinke, M. Scheffler, and C. G. Van de Walle, Appl. Phys. Lett. **95**, 121111 (2009).
[53] K. Shimada, T. Sota, and K. Suzuki, J. Appl. Phys. **84**, 4951 (1998).
[54] J. A. Majewski, M. Stadele, and P. Vogl, MRS Internet J. Nitride Semicond. Res. **1**, 30 (1996).
[55] K. Kim, W. R. L. Lambrecht, B. Segall, and M. van Schilfgaarde, Phys. Rev. B **56**, 7363 (1997).
[56] A. Polian, M. Grimsditch, and I. Grzegory, J. Appl. Phys. **79**, 3343 (1996).
[57] N. W. Ashcroft and N. D. Mermin, *Solid State Physics* (Thomson Learning, Singapore, 1976).
[58] M. Tchounkeu, O. Briot, B. Gil, and R. L. Aulombard, J. Appl. Phys. **80**, 5352 (1996).
[59] W. Shan, T. J. Schmidt, R. J. Hauenstein, J. J. Song, and B. Goldenberg, Appl. Phys. Lett. **66**, 3492 (1995).
[60] S. Kim, I. P. Herman, J. A. Tuchman, K. Doverspike, L. B. Rowland, and D. K. Gaskill, Appl. Phys. Lett. **67**, 380 (1995).
[61] B. Gil, Phys. Rev. B **64**, 201310(R) (2001).
[62] M. R. Wagner, J. H. Schulze, R. Kirste, M. Cobet, A. Hoffmann, C. Rauch, A. V. Rodina, B. K. Meyer, U. Röder, and K. Thonke, Phys. Rev. B **80**, 205203 (2009).